Inorganic Chemistry

Article

pubs.acs.org/IC

Sensitization of Lanthanoid Luminescence by Organic and Inorganic Ligands in Lanthanoid-Organic-Polyoxometalates

Chris Ritchie,[†] Valérie Baslon,[‡] Evan G. Moore,[†] Christian Reber,[‡] and Colette Boskovic*[,†]

[†]School of Chemistry, University of Melbourne, Victoria, 3010, Australia

[‡]Département de Chimie, Université de Montréal, Montréal QC H3C 3J7, Canada

Supporting Information

ABSTRACT: The reaction of terbium and europium salts with the lacunary polyxometalate (POM) $[As_2W_{19}O_{67}(H_2O)]^{14-}$ and 2-picolinic acid (picH) affords the ternary lanthanoid-organic-polyoxometalate (Ln-org-POM) complexes $[Tb_2(pic)(H_2O)_2(B\text{-}\beta\text{-}AsW_8O_{30})_2(WO_2(pic))_3]^{10-}$ (**1**), $[Tb_8(pic)_6(H_2O)_{22}(B\text{-}\beta\text{-}AsW_8O_{30})_4(WO_2(pic))_6]^{12-}$ (**2**), and $[Eu_8(pic)_6(H_2O)_{22}(B\text{-}\beta\text{-}AsW_8O_{30})_4(WO_2(pic))_6]^{12-}$ (**3**). A detailed synthetic investigation has established the conditions required to isolate pure bulk samples of the three complexes as the mixed salts $H_{0.5}K_{8.5}Na$-[**1**]·$30H_2O$, $K_4Li_4H_4$[**2**]·$58H_2O$, and $Eu_{1.66}K_7$[**3**]·$54H_2O$, each of which has been characterized by single crystal X-ray diffraction. Complexes **2** and **3** are isostructural and can be considered to be composed of two molecules of **1** linked through an inversion center with four additional picolinate-chelated lanthanoid centers. When irradiated with a laboratory UV lamp at room temperature, compounds $K_4Li_4H_4$[**2**]·$58H_2O$ and $Eu_{1.66}K_7$[**3**]·$54H_2O$ visibly luminesce green and red, respectively, while compound $H_{0.5}K_{8.5}Na$[**1**]·$30H_2O$ is not luminescent. A variable temperature photophysical investigation of the three compounds has revealed that both the organic picolinate ligands and the inorganic POM ligands sensitize the lanthanoid(III) luminescence, following excitation with UV light. However, considerably different temperature dependencies are observed for Tb(III) versus Eu(III) through the two distinct sensitization pathways.

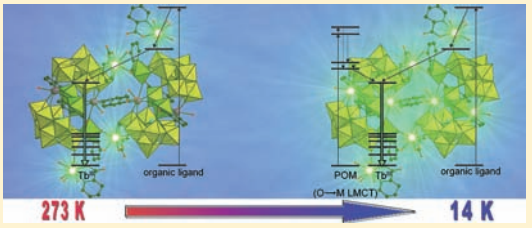

INTRODUCTION

Trivalent lanthanoid (Ln) ions display unique photophysical properties, including sharp and characteristic transitions in the visible or near-infrared regions and long excited-state lifetimes of up to milliseconds. Rare earth phosphors, which are typically classical inorganic solids, have been employed for many years to make use of these properties in fluorescent lamps and cathode ray tubes.[1] More recently, highly luminescent lanthanoid complexes with organic ligands have shown considerable promise for applications in biosensors, fluorescence immunoassays, and as luminescent probes for time-resolved microscopy and bioimaging.[2] The incorporation of these coordination complexes into inorganic or organic−inorganic hybrid hosts, such as organic silicas and ligand-decorated nanoparticles, has afforded organic−inorganic hybrid materials with considerable promise for applications in solid state lighting and for integrated optics and optical telecommunications.[3] Regardless of the host lattice or ligand environment, highly luminescent lanthanoid-based systems require sensitization to overcome the low molar absorption coefficient of the Laporte forbidden f-f transitions (ε < 1−10 L mol^{-1} cm^{-1}). The sensitization process that populates the metal excited states can proceed via a number of mechanisms. In rare earth phosphors the sensitization often involves absorption by the host material, or a second metal ion, with resulting energy transfer through the lattice to the emitting lanthanoid ion. In molecular lanthanoid coordination complexes, the sensitization mostly involves population of the triplet excited state of a conjugated organic ligand, which possesses an intrinsically long lifetime, allowing efficient energy transfer to the emitting lanthanoid ion. The lanthanoid(III) ions with energy levels suitable for emitting visible light are Sm(III), Eu(III), Tb(III), Dy(III), and Tm(III), with Eu(III) (red emission) and Tb(III) (green emission) the most extensively studied because of their longer emissionlifetimes.

Polyoxometalates (POMs) are polynuclear metal−oxo complexes of the early transition metals that are composed of metal-centered MO_n polyhedra linked by shared corners, edges or faces, sometimes with additional heteroatoms incorporated within the cluster.[4] They possess considerable structural and compositional versatility, allowing the tuning of their electronic structure and consequently their functionality. The oxygen-rich surface of defect, or lacunary, POMs renders them excellent inorganic ligands for oxophilic d- and f-block metals, giving rise to a wide variety of coordination complexes. Lanthanoid complexes with POM ligands (Ln-POM complexes)[5] have been reported to display a number of interesting physical properties, including Lewis acid catalytic activity, single-molecule magnetism and luminescence.[6−9]

Ln-POM complexes can also be considered as discrete molecular analogues of rare-earth phosphors. Photoexcitation of the O→M (M = Mo or W) ligand to metal charge transfer (LMCT) bands of the POM ligands can lead to intramolecular

Received: October 31, 2011
Published: December 23, 2011

   dx.doi.org/10.1021/ic202349u | *Inorg. Chem.* 2012, 51, 1142−1151

energy transfer from the O→M excited states to excited energy levels of the lanthanoid(III) ion, thereby sensitizing lanthanoid-(III) emission. Comprehensive studies from Yamase and co-workers have provided considerable insight into the molecular mechanisms of these energy transfer processes.[10−12] The majority of these studies have been performed on Eu-POMs, which have provided the most examples of luminescent Ln-POM complexes. Relatively low emission intensities at room temperature for the other Ln-POMs have been attributed to radiationless deactivation via Ln(IV)−W(V) charge-transfer states for Pr- and Tb-POMs and cross-relaxation based on concentration quenching with a large critical distance for Sm-, Dy-, and Ho-POMs. The emission characteristics of the lanthanoid(III) ion are highly dependent on the nature of the POM ligand, the symmetry and coordination geometry at the lanthanoid center, and the number of aqua coligands. Indeed, POM ligands bound to lanthanoid(III) ions are often polydentate, minimizing the coligation of aqua and similar ligands, which contain high frequency O−H and N−H oscillators that otherwise tend to quench the luminescence. Photoexcitation of the O→M LMCT band of the POM ligand affords emission from the $^5D_0$ and $^5D_1$ excited states of Eu(III) to the ^7F_J (J = 0−4) ground state multiplet for Eu-POM complexes and emission from the $^5D_4$ excited state of Tb(III) to the ^7F_J (J = 0−6) ground state multiplet for Tb-POM complexes (Figure 1).

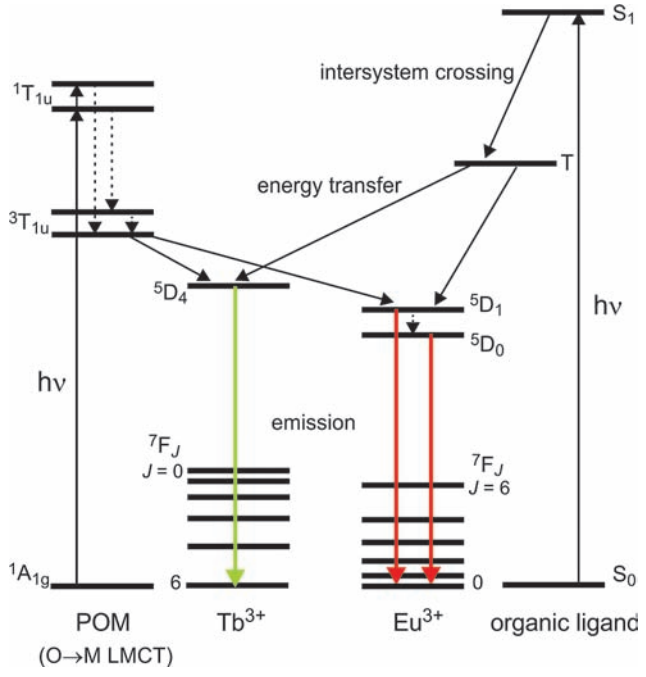

Figure 1. Schematic energy level diagram of relaxation processes for the sensitized emission of Tb(III) and Eu(III) in Ln-org-POM complexes.

The combination of conjugated organic ligands and POM inorganic ligands on single lanthanoid centers to generate "ternary" lanthanoid-organic-POM (Ln-org-POM) complexes affords species with two different routes for sensitizing the lanthanoid luminescence (Figure 1). Early studies of such species have reported sensitized Eu(III)-luminescence arising when (i) a suspension of $[Eu(H_2O)_3(\alpha_2\text{-}P_2W_{17}O_{61})\text{-}(Eu_2(H_2O)_7)_4]_4^{4-}$ in methanol was allowed to interact with a range of organic sensitizing ligands and (ii) phenanthroline and bipyridine were added to acetonitrile solutions of $[EuPW_{11}O_{39}]^{4-}$ and $[Eu(H_2O)_4P_2W_{17}O_{61}]^{7-}$, with the resulting luminescent species proposed to be ternary Eu-org-POM complexes of uncertain identity.[13] Subsequently Eu(III) and Tb(III) luminescence was observed for solid samples inferred to be $[M_4O_{12}Eu(picOH)_3]$ (M = Mo, W, HpicOH = 3-hydroxypicolinic acid) and $[Ln(W_5O_{18})_2(picOH)]$ (Ln = Eu and Tb), although again the luminescent materials were not structurally characterized.[14,15] The first structurally characterized luminescent Ln-org-POM was the polymeric $K_2Na[Eu_3(H_2O)_{14}(HNA)_3\{Eu(H_2O)P_5W_{30}O_{110}\}]\cdot 3H_2O$ (HNA = nicotinic acid).[16] However, in each of the cases described above, the photophysical properties of the compounds were not studied in detail, allowing neither a site-specific determination of the luminescence properties of the different lanthanoid(III) centers nor a delineation of the function of the organic ligand.

As part of an ongoing research program directed at exploring Ln-POMs,[17] we have recently communicated the structurally related dinuclear and octanuclear Tb-org-POM complexes $[Tb_2(pic)(H_2O)_2(B\text{-}\beta\text{-}AsW_8O_{30})_2(WO_2(pic))_3]^{10-}$ (**1**; picH = 2-picolinic acid) and $[Tb_8(pic)_6(H_2O)_{22}(B\text{-}\beta\text{-}AsW_8O_{30})_4(WO_2(pic))_6]^{12-}$ (**2**), which crystallize as the mixed salts $H_{0.5}K_{8.5}Na[\mathbf{1}]\cdot 30H_2O$ and $K_4Li_4H_4[\mathbf{2}]\cdot 58H_2O$.[9] Upon irradiation with a standard UV lamp (λ_{ex} = 254 nm), intense green luminescence was observed for a solid sample of $K_4Li_4H_4[\mathbf{2}]\cdot 58H_2O$, but not for $H_{0.5}K_{8.5}Na[\mathbf{1}]\cdot 30H_2O$. A preliminary room temperature photophysical investigation allowed the identification of the specific terbium centers in complex **2** that are responsible for the luminescence.

Herein we report a more detailed photophysical study of complexes **1** and **2** and the Eu-analogue of **2**, $[Eu_8(pic)_6(H_2O)_{22}(B\text{-}\beta\text{-}AsW_8O_{30})_4(WO_2(pic))_6]^{12-}$ (**3**). This has focused on the temperature-dependence of the lanthanoid-(III) emission following excitation through both the organic picolinate and the inorganic POM ligands, to illuminate the different mechanisms of sensitization.

EXPERIMENTAL SECTION

Synthesis. All manipulations were performed under aerobic conditions. $Na_2WO_4\cdot 2H_2O$ (Riedel-de Haeïn >99%), As_2O_3 (Sigma >99%), $Tb(OAc)_3\cdot H_2O$ (Aldrich 99.9%), $Tb(NO_3)_3\cdot 5H_2O$ (Aldrich 99.9%), $Eu(NO_3)_3\cdot 5H_2O$ (Aldrich, 99.9%), and 2-picolinic acid (Aldrich, 99%) were used as received. The POM precursor $K_{14}[As_2W_{19}O_{67}(H_2O)]$ was prepared as described previously.[18]

$H_{0.5}K_{8.5}Na[Tb_2(pic)(H_2O)_2(B\text{-}\beta\text{-}AsW_8O_{30})_2(WO_2(pic))_3]\cdot 30H_2O$ ($H_{0.5}K_{8.5}Na[1]\cdot 30H_2O$). Solid $Tb(OAc)_3\cdot H_2O$ (0.168 g, 0.500 mmol) was dissolved in water (20 mL), and 2-picolinic acid (0.123 g, 1.00 mmol) was added to the resulting solution. After stirring for 5 min, solid $K_{14}[As_2W_{19}O_{67}(H_2O)]$ (1.32 g, 0.250 mmol) was added. The solution was then stirred for a further 15 min over which time the pH gradually increased to a final value of 3.6. The solution was filtered, covered, and left to stand. After 3−4 weeks well-defined aggregates of plate-like crystals formed that were suitable for X-ray diffraction analysis. Yield after 1 month: 500 mg (31% based on W). Elemental analysis (%) calcd. for $H_{0.5}K_{8.5}Na[\mathbf{1}]\cdot 30H_2O$, $C_{24}H_{80.5}As_2K_{8.5}N_4NaO_{106}Tb_2W_{19}$: C, 4.48; H, 1.26; As, 2.33; K 5.16; N, 0.87; Tb, 4.94; W, 54.26. Found: C, 4.50; H, 0.98; As, 2.29; K, 4.75; Na, 0.34; N, 0.68; Tb, 4.84; W, 54.22. The sodium present in $H_{0.5}K_{8.5}Na[\mathbf{1}]\cdot 30H_2O$ likely results from small amounts of sodium in the $K_{14}[As_2W_{19}O_{67}(H_2O)]$ starting material. Selected IR (KBr, cm^{-1}): 1629 (m), 1477 (w), 1448 (w), 1384 (m), 1350 (m), 1300 (w), 1170 (w), 1055 (w), 951 (m), 862 (s), 798 (s), 764 (m), 698 (s),

$K_4Li_4H_4[Tb_8(pic)_6(H_2O)_{22}(B\text{-}\beta\text{-}AsW_8O_{30})_4(WO_2(pic))_6]\cdot 58H_2O$ ($K_4Li_4H_4[2]\cdot 58H_2O$). Solid $K_{14}[As_2W_{19}O_{67}(H_2O)]$ (1.32 g, 0.250 mmol) was dissolved in water (20 mL), and 2-picolinic acid (0.123

dx.doi.org/10.1021/ic202349u | Inorg. Chem. 2012, 51, 1142−1151

Table 1. Crystallographic Data for the Three Compounds

	$H_{0.5}K_{8.5}Na[\mathbf{1}]\cdot 30H_2O$	$K_4Li_4H_4[\mathbf{2}]\cdot 58H_2O$	$Eu_{1.66}K_7[\mathbf{3}]\cdot 54H_2O$
formula	$C_{24}H_{80.5}As_2K_{8.5}N_4NaO_{106}Tb_2W_{19}$	$C_{72}H_{212}As_4K_4Li_4N_{12}O_{236}Tb_8W_{38}$	$C_{72}H_{196}As_4K_7N_{12}O_{230}Eu_{9.66}W_{38}$
formula weight, g mol^{-1}	6437.54	13763.96	13937.54
space group	$P2_1/c$	$I2/a$	$C2/c$
a/Å	18.1721(2)	32.4845(9)	45.706(3)
b/Å	27.0832(3)	22.5775(6)	22.4012(11)
c/Å	25.6972(2)	41.6085(13)	32.491(2)
β	103.3060(10)	106.041(3)	118.403(9)
V/Å^3	12307.6	29328.3(15)	29262(2)
Z	2	4	4
T/K	130	130	130
ρ_{calc}/g cm^{-3}	3.523	3.065	3.169
μ/mm^{-1}	41.808	37.896	43.625
reflns measd	68857	44578	37504
unique reflns	22167	15296	15569
data/restraints/parameters	22167/0/1485	15296/2/1464	37504/0/802
R_{int}			
R_1 [$I > 2\sigma(I)$]	0.0533	0.0580	0.0598
wR_2 (all data)	0.0973	0.1401	0.1328
goodness-of-fit on F^2	0.971	1.057	0.712
$\Delta\rho_{max,min}$/e Å^{-3}	2.973, − 2.834	2.597, −3.420	2.51, −2.36

g, 1.00 mmol) was added to the resulting solution. Solid LiCl (0.85 g, 20 mmol) was added until the solution became clear at 30 °C. Solid $Tb(NO_3)_3{\cdot}5H_2O$ (0.218 g, 0.500 mmol) was added to the resulting solution, which was then heated to 70 °C until all reagents fully dissolved, at which point the pH was 3.9. The solution was removed from the heat, cooled to room temperature, covered and left to stand. After 3−4 weeks well-defined rod-shaped crystals, suitable for X-ray diffraction analysis, were collected. Yield after 1 month: 300 mg (18% based on W). Elemental analysis (%) calcd. for $K_4Li_4H_4[\mathbf{2}]\cdot 58H_2O$, $C_{72}H_{212}As_4K_4Li_4N_{12}O_{236}Tb_8W_{38}$: C, 6.28; H, 1.55; As, 2.18; K, 1.14; Li, 0.20; N, 1.22; Tb, 9.24; W, 50.76. Found: C, 6.55; H, 1.39; As, 2.17; K, 1.13; Li, 0.20; N, 1.20; Tb, 8.61; W, 49.70. Selected IR (KBr, cm^{-1}): 1633 (m), 1568 (m), 1478 (w), 1447 (w), 1384 (m), 1300 (w), 1054 (w), 947 (m), 855 (s), 802 (m), 760 (m), 698 (s).

$Eu_{1.66}K_7[Eu_8(pic)_6(H_2O)_{22}(B\text{-}\beta\text{-}AsW_8O_{30})_4(WO_2(pic))_6]\cdot 54H_2O$ ($Eu_{1.66}K_7[\mathbf{3}]\cdot 54H_2O$). Solid $K_{14}[As_2W_{19}O_{67}(H_2O)]$ (1.32 g, 0.250 mmol) was dissolved in water (20 mL), and 2-picolinic acid (0.123 g, 1.00 mmol) was added to the resulting solution. The solution was then heated to 40 °C, $Eu(NO_3)_3{\cdot}5H_2O$ (0.214 g, 0.500 mmol) added, and the reaction mixture further heated to 70 °C until all reagents fully dissolved, at which point the pH of the solution was 3.9. The solution was removed from the heat, cooled to room temperature, covered and left to stand. After 3−4 weeks well-defined rod-shaped crystals, suitable for X-ray diffraction analysis, were collected. Yield after 1 month: 400 mg (23% based on W). Elemental analysis (%) calcd. for $Eu_{1.66}K_7[\mathbf{3}]{\cdot}54H_2O$, $C_{72}H_{196}As_4K_7N_{12}O_{230}Eu_{9.66}W_{38}$: C, 6.34; H, 1.51; As, 2.22; K, 2.01; N, 1.23; Eu, 10.78; W, 48.56. Found: C, 6.43; H, 1.44; K, 2.13; N, 1.00; Eu, 10.82; W, 50.02. Selected IR (KBr, cm^{-1}): 1628 (m), 1584 (m), 1566 (m), 1478 (w), 1448 (w), 1384 (m), 1300 (w), 1261 (w), 1054 (w), 947 (m), 861 (s), 795 (s), 760 (m), 697 (s).

X-ray Data Collection and Structure Solution. The crystallographic data (Table 1) for compounds $H_{0.5}K_{8.5}Na[\mathbf{1}]\cdot 30H_2O$ and $K_4Li_4H_4[\mathbf{2}]\cdot 58H_2O$ were collected at 130 K on a Gemini Oxford Diffractometer using graphite-monochromated Cu Kα radiation (1.54184 Å), and the data for compound $Eu_{1.66}K_7[\mathbf{3}]\cdot 54H_2O$ were collected on a Xcalibur Sapphire3 Oxford Diffractometer using graphite-monochromated Cu Kα radiation (1.54184 Å). Empirical absorption corrections were carried out using a multifaceted crystal model and the ABSPACK routine within the CrysAlis software package. All three structures were solved by direct methods and refined by the full-matrix least-squares method on F^2 using the SHELXTL-97 crystallographic package. During the refinement process it was not possible to crystallographically locate all the solvent water molecules or cations present in the formulas assigned to the three compounds. In $Eu_{1.66}K_7[\mathbf{3}]\cdot 54H_2O$ the additional europium countercations were located as three independent disordered Eu(III) metal centers, and their occupancies determined using the SHELX EADP command. Assignment of these atomic positions as europium is strongly supported by an excellent fit of the elemental analysis data for $Eu_{1.66}K_7[\mathbf{3}]\cdot 54H_2O$. All other values were determined based upon the combination of charge balance requirements, crystallographic observations, and elemental analyses. Hydrogen atoms could not be located from the electron density map.

Photoluminescence. Room temperature steady state luminescence emission and excitation spectra were acquired with an emission spectrometer (FluoroLog-3-11, HORIBA Jobin Yvon) using a 450 W Xe Arc lamp as the light source. An Acton Trivista 500i spectrometer with a mercury lamp was used to measure variable temperature steady state luminescence emission spectra with UV excitation (313 nm, 285 nm), with the samples cooled in a helium gas cryostat. The CCD camera acquires the regions above and below 500 nm separately. All luminescence transitions presented in the following are in the same wavelength range, with the exception of the Tb(III) $^5D_4\rightarrow{}^7F_6$ transition at 490 nm, the intensity of which might therefore not be precisely comparable to those of the other Tb(III) f-f luminescence bands.

Time resolved experiments were performed with a nanosecond laser setup, based on a Nd:YAG (Continuum NY-61-10, Coherent) pumped OPO system (Casix BBO, Shanghai Uniwave Technologies) tuned to 560 nm as the light source (frequency doubled to give λ_{ex} = 280 nm), a 0.3 m triple grating monochromator (SpectraPro 300i, Acton Instruments) for spectral selection, and a PMT tube (R928P, Hamamatsu) as the detector, which was sampled directly using a 500 MHz digital oscilloscope (TDS520, Tektronix). The instrument response function (IRF) for this setup was measured to be about 12 ns at fwhm. Each resulting trace contained at least 1000 data points, and was averaged over 1000 shots. Data analysis was performed using a commercially available software package (Igor, Version 6.1.2.1, Wavemetrics), and the quality of the fit was assessed from the chi-squared χ^2 value and by inspection of the weighted residuals. Reported values are the averages of three independent measurements.

Other Measurements. Infrared spectra (KBr disk) were recorded on a Bruker Tensor 27 FTIR spectrometer. Elemenatal analyses were performed by Chemical and Microanalytical Services, Belmont, Australia and the Microanalytical Unit, Research School of Chemistry, Australian National University, Australia.

dx.doi.org/10.1021/ic202349u | Inorg. Chem. 2012, 51, 1142−1151

RESULTS AND DISCUSSION

Syntheses. All three compounds were synthesized from reaction mixtures containing $[As_2W_{19}O_{67}(H_2O)]^{14-}$, LnX_3 (X = AcO^- or NO_3^-) and picH in the respective stoichiometric ratios of 1:2:4. The nature of the final product that crystallizes from solution in each case appears to depend on four factors: (i) the counterion of the lanthanoid salt used as a starting material, (ii) the final pH of the solution prior to crystallization, (iii) whether or not the reaction mixture was heated during the course of the reaction, and (iv) the presence or absence of additional lithium cations. The dinuclear terbium complex **1** is obtained when $Tb(OAc)_3$ is employed as a starting material, the reaction solution is not heated, and the final pH prior to crystallization is 3.6. In contrast the octanuclear complexes **2** and **3** are obtained from lanthanoid nitrate salts, with heating of the reaction mixture and final solution pH values of 3.9. Extra lithium cations are required to obtain a pure bulk sample of **2** as the mixed salt $K_4Li_4H_4[\mathbf{2}]\cdot 58H_2O$, with the lithium cations likely enhancing the solubility of the POM reaction intermediates to allow formation of the final product. However, an analogous approach with europium does not afford an isomorphous material, with complex **3** crystallizing in the absence of lithium as the mixed salt $Eu_{1.66}K_7[\mathbf{3}]\cdot 54H_2O$. It seems likely that the dinuclear and octanuclear complexes are in equilibrium, as deviation from the precise conditions required to crystallize pure bulk samples of each of the compounds affords mixtures of the di- and octanuclear species.

Balanced chemical reactions for the formation of the polyanions **1**−**3** are presented in eqs 1 and 2.

$$[As_2W_{19}O_{67}(H_2O)]^{14-} + 2\,Tb^{3+} + 4\,pic^- + 2H^+ \rightarrow [Tb_2(pic)(H_2O)_2(B\text{-}\beta\text{-}AsW_8O_{30})_2(WO_2(pic))_3]^{10-} \quad (1)$$

$$2\,[As_2W_{19}O_{67}(H_2O)]^{14-} + 8\,Ln^{3+} + 12\,pic^- + 18\,H_2O + 4\,H^+ \rightarrow [Ln_8(pic)_6(H_2O)_{22}(B\text{-}\beta\text{-}AsW_8O_{30})_4(WO_2(pic))_6]^{12-} \quad (2)$$

While the POM/lanthanoid/picolinate ratios of 1:2:4 employed in all of the syntheses is reflected exactly in the composition of dinuclear complex **1**, the final ratio evident in both octanuclear complexes **2** and **3** is 1:4:6. The difference between the ratios in the reaction media and the final product is the likely cause of the lower yield obtained for the syntheses of **2** and **3**. However, modification of the synthetic method to employ reaction ratios that reflect the composition of the final products does not improve the yields of **2** and **3**. This probably reflects the complex equilibria that exist in these multicomponent reaction mixtures, where the product that ultimately crystallizes is simply the least soluble species. It is notable that all three compounds only begin to form after the reaction solutions are left to stand for several weeks, indicating that they are thermodynamic rather than kinetic products.

It is of interest to compare the syntheses of complexes **1**−**3**, with that of a three-dimensional framework material $[K_2\{Dy(H_2O)_3\}_2\{As_2W_{19}O_{68}\}\{WO_2(pic)\}_2]^{6-}$ (**4**) that we have recently reported, which is prepared using the same reaction stoichiometry and pH but double the ionic strength.[17c] Complex **4** crystallizes as a potassium salt within a couple of days, from a slightly more acidic solution (pH 3.4) which has not been heated, suggesting that **4** is likely a kinetic product of the same reaction. Insight into the relationship between the structure of the final products and the synthetic conditions can be gained by considering the structures of the POM fragments evident in these compounds relative to that of the POM precursor $[As_2W_{19}O_{67}(H_2O)]^{14-}$. While the POM building blocks of complexes **1**−**3** are $\{B\text{-}\beta\text{-}AsW_8O_{30}\}$ units that arise following multiple structural dissociation and isomerization steps (Scheme 1), the $\{As_2W_{19}O_{68}\}$ POM building block in **4** arises from a relatively simple structural modification of the POM precursor.[8] All four complexes incorporate $\{WO_2(pic)\}$ fragments, consistent with the $[As_2W_{19}O_{67}(H_2O)]^{14-}$ precursor fragmenting to afford $\{B\text{-}\alpha\text{-}AsW_9O_{33}\}$ units and free tungstate that is scavenged by picolinate ligands. The greater ionic strength in the reaction solution that affords **4** gives rise to the rapid crystallization of the relatively insoluble $\{As_2W_{19}O_{68}\}$-containing **4**, driving the equilibrium between the $\{B\text{-}\alpha\text{-}AsW_9O_{33}\}$ and $\{B\text{-}\beta\text{-}AsW_9O_{33}\}$ isomers back toward $\{B\text{-}\alpha\text{-}AsW_9O_{33}\}$ and ultimately $\{As_2W_{19}O_{68}\}$ structural fragments. It is only in much more dilute reaction solutions that crystallization of $\{As_2W_{19}O_{68}\}$-containing species is prevented and there is time for the formation of the $\{B\text{-}\beta\text{-}AsW_8O_{30}\}$ building blocks evident in **1**−**3**.

Scheme 1

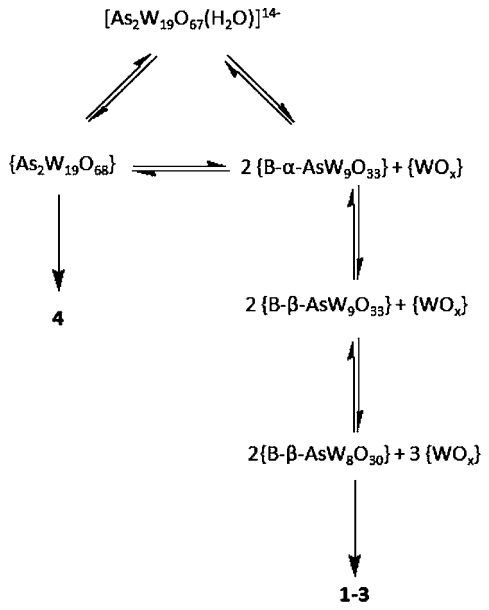

Structures. Selected single crystal X-ray data for the three compounds are available in Table 1 and structural representations of complexes **1**−**3** are available in Figure 2. Compound $H_{0.5}K_{8.5}Na[\mathbf{1}]\cdot 30H_2O$ crystallizes in the monoclinic space group $P2_1/c$, with the asymmetric unit containing the entire polyanion. Compounds $K_4Li_4H_4[\mathbf{2}]\cdot 58H_2O$ and $Eu_{1.66}K_7[\mathbf{3}]\cdot 54H_2O$ crystallize in the monoclinic space groups $I2/a$ and $C2/c$, respectively, with the asymmetric unit containing half of the polyanion in each case.

The structure of complex **1** can be described as two $\{B\text{-}\beta\text{-}AsW_8O_{30}\}$ units that are orientated at 180° with respect to each other, linked by Tb1 acting as a "hinge". The space between the hinged $\{B\text{-}\beta\text{-}AsW_8O_{30}\}^{9-}$ units is occupied by a second Tb center (Tb2) and three $\{WO_2(pic)\}$ units, all of which are linked by corner-sharing to each other and the $\{B\text{-}\beta\text{-}AsW_8O_{30}\}$ units. The structure of the isostructural octanuclear Ln complexes **2** (Ln = Tb) and **3** (Ln = Eu) can in turn be considered as two molecules of **1**, linked by two crystallographically equivalent $\{Ln(pic)(H_2O)_3\}$ moieties (Ln3), which are ultimately related by inversion symmetry. An additional two lanthanoid centers (Ln4) are also grafted to the surface of the

dx.doi.org/10.1021/ic202349u | Inorg. Chem. 2012, 51, 1142−1151

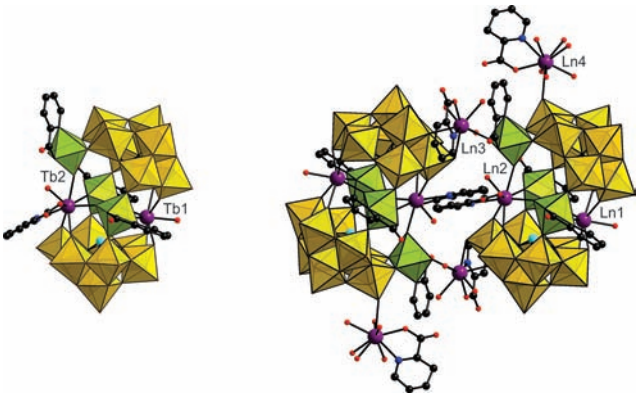

Figure 2. Combined polyhedral/ball-and-stick representation of the polyanions in (left) **1** and (right) **2** (Ln = Tb) and **3** (Ln = Eu). Color code: WO_6 octahedra ($\{AsW_8O_{30}\}$ units), yellow; WO_6 octahedra ($\{WO_2(pic)\}$ units), green; Ln, violet; As, pale blue; C, black; N, dark blue; O, red.

complex as peripheral picolinate chelates. In all three complexes the bond lengths are consistent with trivalent lanthanoid centers (Supporting Information, Table S1), with previous magnetic studies on $H_{0.5}K_{8.5}Na[\mathbf{1}]\cdot 30H_2O$ and $K_4Li_4H_4[\mathbf{2}]\cdot 58H_2O$ also indicative of Tb(III) in these complexes.[9]

Complexation of multiple metal centers between two lacunary POM fragments is a common occurrence; however, the arrangement evident in **1**−**3** is unlike any reported previously. Generally compounds of this type fit into one of the four main "sandwich POM" structural classes, namely, Knoth, Hervé, Weakley, or Krebs.[19] Recently, however, more structurally diverse architectures with multiple 3d metal centers coordinated into the asymmetric lacunary site of polyoxotungstates have been reported. Some of these include the $\{XW_8O_{30}\}$ or $\{XW_8O_{31}\}$ (X = Si, Ge, and P) tetravacant lacunary Keggin POMs coordinated to multiple Cu(II), Co(II), and Mn(II) centers.[20] However, to the best of our knowledge the complexes reported herein remain the only examples to contain lanthanoid ions complexed by $\{XW_8O_{30}\}$ polyanions.

An intriguing structural feature of **1**−**3** (and **4**) is the chelation of picolinate ligands to the tungsten centers through the pyridyl nitrogen and one of the carboxylate donor atoms. Complexes **1**−**4** are the only examples of coordination of POM tungsten centers to nitrogen donor atoms, because of the preference of the hard W(VI) ions for hard oxygen donor atoms. It is for this reason that several research groups wishing to incorporate pyridyl containing ligands into POM-based materials introduce 3d metals or reduced Mo/V ions into polyoxotungstates.[21] Each of the tungsten centers in the $\{WO_2(pic)\}$ units possess a long W−N(pyridyl) coordinate bond in the range 2.22−2.34 Å, leading to the invariable assignment of the trans ligand as a short tungsten to oxygen bond with significant double bond character. This chemical requirement has a profound impact on the structures that can be formed in the presence of these building blocks, as exemplified by the inability to regenerate the $\{B\text{-}\beta\text{-}AsW_9O_{33}\}$ motif (Supporting Information, Figure S1), with this bonding pattern clearly favoring the alternating arrangement of tungsten and lanthanoid centers evident in **1**−**3**. The secondary coordination environment surrounding the non-sandwiched $\{WO_2(pic)\}$ group is different in **1** compared to **2** and **3**. In complex **1** the oxo group located cis to the nitrogen of the picolinate ligand that is not involved in bonding to the $\{AsW_8O_{30}\}$ fragment is coordinated to a potassium cation (Supporting Information, Figure S2), whereas in **2** and **3** coordination occurs to an additional lanthanoid center (Ln3), which in turn acts as the sole covalent bridge linking the two molecules of **1** to make **2**.

Sandwiched between the two $\{AsW_8O_{30}\}$ units in **1**−**3** are $\{Ln(H_2O)\}$ (Ln1) and $\{Ln(pic)(H_2O)\}$ (Ln2) units. With 7-coordinate Ln1 and 8-coordinate Ln2 displaying coordination geometries best approximated as distorted capped trigonal prismatic and square antiprismatic, respectively (Figure 3). The lanthanoid center Ln1 is coordinated to a single terminal aqua ligand and has six corner-sharing Ln−O−W linkages, with Ln−O−W angles in the range 124−170° for the three compounds (Supporting Information, Table S1). The lanthanoid center Ln2 is chelated by a picolinate ligand and has a single aqua ligand and five corner-sharing Ln−O−W linkages, with Ln−O−W angles in the range 150−161°. The linking center Ln3 and peripheral center Ln4 are also each chelated by a picolinate ligand in an analogous manner to Ln2, as $\{Ln(pic)(H_2O)_3\}$ and $\{Ln(pic)(H_2O)_6\}$ fragments, respectively (Figure 3). While the 8-coordinate Ln3 also displays a distorted square antiprismatic coordination geometry, 9-coordinate Ln4 is best described as distorted capped trigonal prismatic. Lanthanoid center Ln3 has three terminal aqua ligands, two edge-sharing and two corner sharing Ln−O−W linkages. The edge-sharing linkages are associated with more acute Ln−O−W angles of 93−107°, while the corner-sharing linkage has Ln−O−W angles of 142−163° for complexes **2** and **3**. Lanthanoid center Ln4 with six aqua ligands, is connected to the $\{AsW_8O_{30}\}$ portion of the complex through a single Ln−O−W linkage, with Ln−O−W angles in the range 147−148°. Complexes **2** and **3** are isostructural, with the slightly longer Eu−O/N versus Tb−O/N bond lengths consistent with the larger ionic radius of europium(III) versus terbium(III).

Multiple well-defined noncovalent intramolecular interactions stabilize the structures of complexes **1**−**3**, including

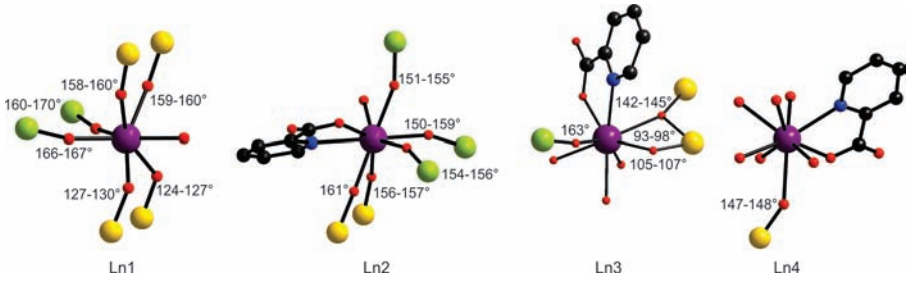

Figure 3. Ln coordination environments and Ln−O−W bond angles in **1**−**3**. Color code as per Figure 2.

dx.doi.org/10.1021/ic202349u | *Inorg. Chem.* 2012, 51, 1142−1151

numerous hydrogen bonding and C−H···π interactions (Supporting Information, Figure S3). This is particularly evident as O−H···O hydrogen bonds between the lanthanoid aqua ligands and either the POM oxo ligands or the noncoordinated carboxylic oxygen atoms of the picolinate ligands. In addition, C−H···π interactions are evident between the π system of the picolinate ligand coordinated to Ln2 and the α-proton next to the pyridyl nitrogen on the picolinate ligand coordinated to Ln3.

Intermolecular interactions are also important for the three compounds (Supporting Information, Figures S2, S4 and S5), including the coordination of potassium countercations to the POMs. This is particularly the case for complex **1**, where these potassium ions occupy binding sites that are occupied by the Tb3 and Tb4 centers in complex **2**. A number of intermolecular hydrogen bonds are also evident, in addition to intermolecular $\pi-\pi$ stacking between picolinate ligands.

Infrared Spectroscopy. The infrared spectra of compounds $H_{0.5}K_{8.5}Na[\mathbf{1}]\cdot 30H_2O$, $K_4Li_4H_4[\mathbf{2}]\cdot 58H_2O$, and $Eu_{1.66}K_7[\mathbf{3}]\cdot 54H_2O$ are all very similar with only slight shifts in the position of the bands (Supporting Information, Figure S5). All compounds show broad peaks at about 3400 and 1600 cm^{-1}, which are attributed to the stretching and bending modes of lattice and coordinated water molecules. A pattern of three peaks in the range 2850−2950 cm^{-1} are due to the C−H stretches. A characteristic peak for the polyanions at about 948 cm^{-1} can be assigned to the W═O stretching vibration, peaks at about 859 and 798 cm^{-1} correspond to the two types of W−O−W stretching vibrations and the peak at 698 cm^{-1} can be assigned to the W−O(-As) stretch.[22] The picolinate carboxylate stretching vibrations are observed at about 1384 and 1630 cm^{-1}, for the symmetric and antisymmetric stretches, respectively, with the latter band overlapping with the O−H bend of free and coordinated water.[23] Bands due to carboxylate bending vibrations are also evident in the range 630−750 cm^{-1}, although they overlap with some of the POM stretches. The stretching vibrations of the heterocyclic picolinate ring ν(C═C and C═N) are evident in the range 1450−1600 cm^{-1}.[23]

Photoluminescence. Upon irradiation with a standard UV lamp (λ_{ex} = 254 nm) at room temperature, intense Tb(III)-based green and Eu(III)-based red luminescence is observed for solid samples of $K_4Li_4H_4[\mathbf{2}]\cdot 58H_2O$ and $Eu_{1.66}K_7[\mathbf{3}]\cdot 54H_2O$, respectively, with no visible luminescence apparent for $H_{0.5}K_{8.5}Na[\mathbf{1}]\cdot 30H_2O$. Given the partial congruence of the terbium coordination sites in complexes **1** and **2**, this observation immediately suggests that terbium centers Tb1 and Tb2 are not luminescent at room temperature, with the visible luminescence of complex **2** ascribed to Tb3 and/or Tb4. To gain insight into the potentially complicated luminescence behavior of complexes **1**−**3**, variable temperature photophysical measurements were performed, focusing on the effects of sensitizing the lanthanoid(III) luminescence via excitation at wavelengths corresponding to absorption of either the picolinate or the POM ligands.

By monitoring the room temperature Eu(III) emission of solid $Eu_{1.66}K_7[\mathbf{3}]\cdot 54H_2O$ at 615 nm, the excitation spectrum was collected (Figure 4a). This shows peak maxima at about 279 and 315 nm, which can be attributed to absorption by the coordinated organic picolinate and inorganic POM ligands, respectively, resulting in subsequent Eu(III)-centered emission.[10−12,23]

The corresponding variable temperature emission spectra for solid $Eu_{1.66}K_7[\mathbf{3}]\cdot 54H_2O$ are shown in Figures 4b and 4c.

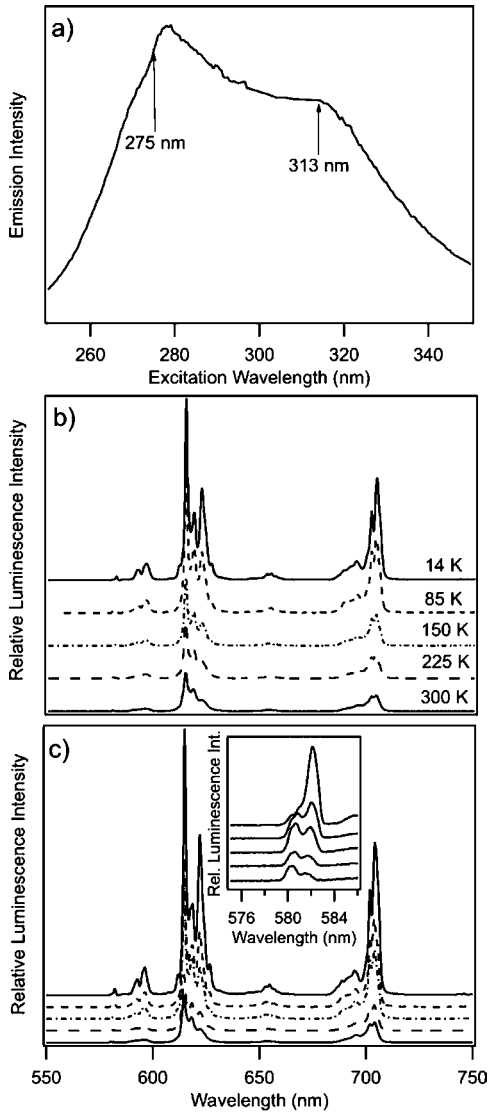

Figure 4. (a) Excitation (λ_{emiss} = 615 nm), (b) temperature-dependent luminescence (λ_{ex} = 275 nm), and (c) temperature-dependent luminescence (λ_{ex}= 313 nm) spectra for solid $Eu_{1.66}K_7[\mathbf{3}]\cdot 54H_2O$ with spectra shown at 14, 85, 150, 225, and 300 K (top to bottom). Inset to (c): temperature dependence of the highest-energy luminescence transitions.

Spectra were measured with excitation wavelengths of 275 and 313 nm, which correspond to excitation through the picolinate and POM ligands, respectively. The 14 K emission spectra of $Eu_{1.66}K_7[\mathbf{3}]\cdot 54H_2O$ at both excitation wavelengths display characteristic transitions from the $^5D_0$ excited states of Eu(III) to the ^7F_J manifold. The apparent peak maxima are at about 582, 590, 620, 650, and 700 nm for the J = 0, 1, 2, 3, and 4 transitions, respectively. In europium(III) compounds the $^5D_0 \rightarrow {}^7F_0$ transition is a singlet for each emitting site. Our best resolved spectrum at 14 K (λ_{ex}= 313 nm) shows a dominant peak at 582.0 nm with a width at half height of 1 nm, and a weaker maximum at 580.8 nm, higher in energy by 35 cm^{-1}. This small separation corresponds to the energy difference among the different europium emitting sites, indicating that the coordination environment is similar for the two or more emitting sites. The two peak maxima are also observed in the spectra measured with 275 nm excitation. In general for Eu(III)-luminescence, the magnetic-dipole allowed

dx.doi.org/10.1021/ic202349u | Inorg. Chem. 2012, 51, 1142−1151

$^5D_0 \rightarrow {}^7F_1$ transition is little affected by the coordination geometry, whereas the intensity of the electric-dipole allowed $^5D_0 \rightarrow {}^7F_2$ transition depends strongly on the coordination geometry and metal−ligand covalency. For compound $Eu_{1.66}K_7[\mathbf{3}]\cdot 54H_2O$ the hypersensitive $^5D_0 \rightarrow {}^7F_2$ transition is relatively intense with $I(^5D_0 \rightarrow {}^7F_2)/I(^5D_0 \rightarrow {}^7F_1)$ ratios of about 12 and 10 for λ_{ex} = 275 and 313 nm, respectively, suggesting low local symmetry at the emitting sites.

As the temperature is increased from 14 K to above 150 K the intensity of the weak, high-energy, peak of the $^5D_0 \rightarrow {}^7F_0$ transition observed at 580.8 nm for $Eu_{1.66}K_7[\mathbf{3}]\cdot 54H_2O$ increases compared to the more intense, lower energy peak at 582 nm for both excitation wavelengths, suggesting that the emission from the higher-energy site/s gains intensity through thermal population and energy transfer processes. At room temperature, the higher energy peak is dominant, a reversal of the intensity distribution at 14 K. Otherwise, the general trend is that the intensity of all transitions decreases as the temperature is increased up to 300 K, with very similar I_{14K}/I_{300K} intensity ratios of about 5 and 6 for the $^5D_0 \rightarrow {}^7F_1$ transitions for λ_{ex} = 275 and 313 nm, respectively. This is associated with a general increase in line width, but no significant shift in peak position, indicating the absence of major structural changes with temperature. The temperature dependence of the luminescence intensity for all excitation wavelengths is similar, possibly because of efficient energy transfer among the Eu(III) sites, preventing the measurement of sensitization through POM absorption to the nearest Eu(III) site.

Room temperature time-resolved emission profiles were also collected for $Eu_{1.66}K_7[\mathbf{3}]\cdot 54H_2O$ at 615 nm, with λ_{ex} = 280 nm. Multiexponential decay behavior was observed, which was not unexpected given the presence of four different Eu(III) centers in each complex. Fitting the decay profiles gave satisfactory agreement to a biexponential function, with lifetime values of τ_1 = 195 ± 13 μs (19%) and τ_2 = 393 ± 3 μs (82%), which are consistent with expected values for hydrated complexes of Eu(III).[24,25] The 80:20 ratio suggests a significant difference in the intensities of the two different emitting sites. As Eu(III) displays a considerable sensitivity to quenching of the luminescence by coordinated aqua ligands, this likely indicates differing numbers of such ligands on the two sites.

The different spectroscopic experiments suggest the presence of at least two different emitting Eu(III) centers in $Eu_{1.66}K_7[\mathbf{3}]\cdot 54H_2O$ across the temperature range 14−300 K, regardless of whether the luminescence is sensitized by excitation through the organic picolinate or inorganic POM ligands. The emission intensities display significant temperature dependencies for both excitation wavelengths. Variable temperature spectroscopic studies of Eu-POMs have revealed the temperature dependence of the Eu(III) emission intensity upon excitation into the O→M LMCT bands is always greater than under excitation of the f-f bands, because of thermal relaxation of the O→M LMCT states competing with energy transfer to the Eu(III) ion. However, the extent of temperature dependence upon excitation into the O→M LMCT bands depends on both the Eu−O−M angles at the emitting site and the M−O−M angles within the POM ligand.[10,12] Thermal deactivation of the O→M LMCT states is associated with electron hopping delocalization within the POM ligand, which depends on the configuration of both M−O−M and Eu−O−M linkages. Photoexcitation into the O→M LMCT bands allows the d^1 electron to hop to the Eu(III) site via the Eu−O−M linkage when the Eu−O−M angles are around 150° because of fπ-pπ-dπ orbital mixing in the Eu−O−M linkage, similar to dπ-pπ-dπ mixing that occurs at corner-shared MO_6 octahedra with M−O−M bond angles of around 150°. Thus Eu-POMs with Eu−O−M angles of greater than 150° display a significant decrease in emission intensity with increasing temperature, while Eu-POMs with only edge-shared MO_6 octahedra and Eu−O−M angles of around 100° show little temperature dependence of the emission intensity because of localization of the d^1 electron on the MO_6 octahedra. A decrease of the intensity of Eu(III) emission with increasing temperature has also been observed for complexes with only organic ligand sensitizers and ascribed to nonradiative relaxation from the $^5D_0$ state because of crossover to a low-lying LMCT state.[24] Typically an increase in line width is also observed with temperature, particularly for less rigid structures.[23]

The structural complexity of **3** renders a precise assignment of the luminescence to specific europium sites impossible. Three of the four europium centers, Eu2, Eu3, and Eu4 (Figure 3), coordinate to picolinate ligands and are thus candidates as emitting sites following excitation through the organic chromophore, while potentially all four centers may display luminescence following excitation through the POM. Europium centers Eu1, Eu2, Eu3, and Eu4 have one, one, three, and six aqua ligands, respectively, which can give rise to quenching of Ln(III) emission, shortening luminescence lifetimes through nonradiative relaxation processes involving OH oscillators.[26] They also have four, six, one, and one Eu−O−W bridging angles greater than 145°, respectively, which are associated with marked temperature dependence of the emission following excitation into the POM. Only Eu3 has two Eu−O−W bridging angles in the range 95−110°, because of edge-sharing, which are associated with little temperature dependence of the emission. The lack of luminescence of Tb-containing **1** indicates that the emitting centers in **2** are Tb3 and Tb4, and it is likely the equivalent Eu3 and Eu4 sites in isostructural **3** are also emitting, at least following excitation through the picolinate ligand. The shorter luminescence lifetime is assigned to Eu4, with six aqua ligands to quench the luminescence, while the longer lifetime is assigned to Eu3, which only has three aqua ligands.

By monitoring the room temperature Tb(III) emission of $K_4Li_4H_4[\mathbf{2}]\cdot 58H_2O$ at 490 nm, the excitation spectrum was also collected, showing a peak maximum at about 276 nm and a smaller shoulder at slightly lower wavelength, both of which we attribute to absorption by the coordinated picolinate ligands, resulting in subsequent Tb(III)-centered emission (Figure 5a).[23] The absence of any other excitation peaks in the UV region indicates that in contrast to the europium analogue, sensitization of the Tb(III) ions at room temperature proceeds solely via the organic chromophores, and does not involve POM-centered LMCT states. This is in accordance with results from Yamase et al., who have shown that room temperature sensitization via the latter pathway is not efficient for Tb(III) because of radiationless deactivation involving Tb(IV)−W(V) charge transfer states.[10]

The 14 K emission spectra of $K_4Li_4H_4[\mathbf{2}]\cdot 58H_2O$ at excitation wavelengths of 275 and 313 nm both display characteristic transitions from the $^5D_4$ excited state of Tb(III) to ground state ^7F_J manifold (Figures 5b and 5c), consistent with excitation through both picolinate and POM ligands at this temperature. The apparent peak maxima are at about 492, 544, 583, 622, 650, 670, and 680 nm for the J = 6, 5, 4, 3, 2, 1, and 0

dx.doi.org/10.1021/ic202349u | Inorg. Chem. 2012, 51, 1142−1151

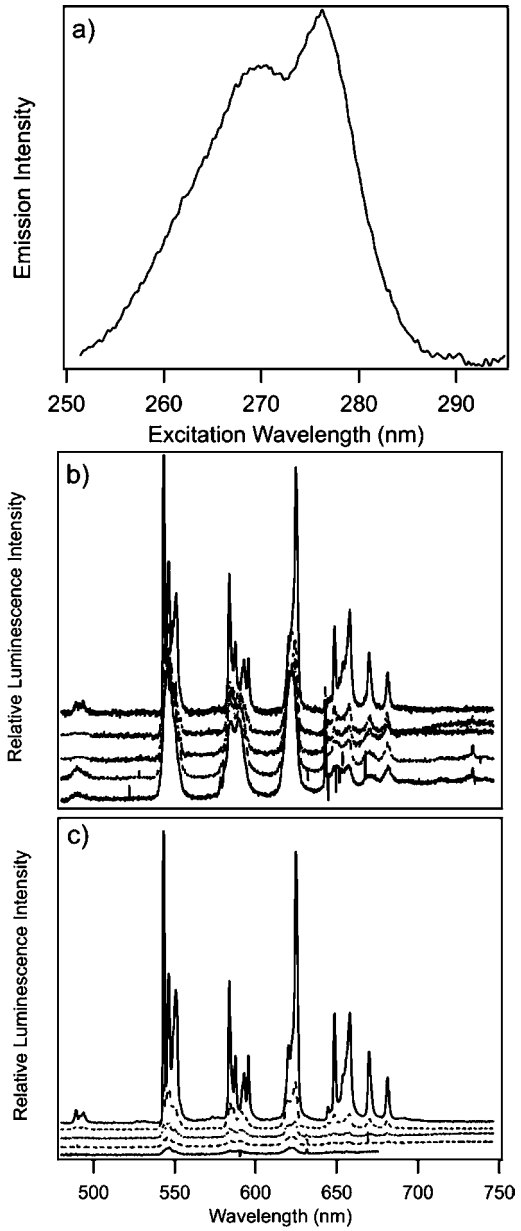

Figure 5. (a) Excitation (λ_{emiss} = 490 nm), (b) temperature-dependent luminescence (λ_{ex} = 275 nm), and (c) temperature-dependent luminescence spectra (λ_{ex} = 313 nm) for solid $K_4Li_4H_4[\mathbf{2}]\cdot 58H_2O$ with spectra shown at 14, 85, 150, 225, and 300 K (top to bottom).

transitions, respectively. For terbium(III) the hypersensitive electric-dipole allowed transitition is $^5D_4 \rightarrow {}^7F_6$, which can be compared with the environment-insensitive magnetic-dipole allowed $^5D_4 \rightarrow {}^7F_5$ transition. For $K_4Li_4H_4[\mathbf{2}]\cdot 58H_2O$ at 14 K, $I(^5D_4 \rightarrow {}^7F_5)/I(^5D_4 \rightarrow {}^7F_6)$ intensity ratios of about 0.05 are determined for both λ_{ex} = 275 and 313 nm, again suggesting low local symmetry at the emitting sites.

As the temperature is increased from 14 to 300 K, the intensity of all transitions again decreases for both excitation wavelengths. However the change with temperature is much more marked for λ_{ex} = 313 versus λ_{ex} = 275 nm, as illustrated in Figure 5. The integrated luminescence intensity decreases by a factor of 30 between 14 and 300 K for the spectra measured with an excitation wavelength of 313 nm, resulting in very weak luminescence at room temperature, but only by a factor of 2 for the spectra measured with an excitation wavelength of 275 nm over the same temperature range. This is consistent with the absence of a peak due to POM absorption in the 300 K excitation spectrum and indicates a much greater temperature sensitivity for excitation through the POM than compared with excitation through the picolinate ligand, as has been observed previously by Yamase et al.[12] The decrease in intensity is again accompanied by an increase in line width, but no significant shift in wavelength.

Room temperature time-resolved emission profiles were collected for $K_4Li_4H_4[\mathbf{2}]\cdot 58H_2O$ at 490 nm, with λ_{ex} = 280 nm. A multiexponential decay behavior was again observed, which could be fit satisfactorily to a biexponential function, with lifetime values of τ_1 = 58 ± 2 μs (51%) and τ_2 = 274 ± 10 μs (49%), consistent with expected values for hydrated complexes of Tb(III).[27] The approximately equal contributions for the two emitting sites suggests that the metal-centered emission intensities are similar for the two sites, in contrast to $Eu_{1.66}K_7[\mathbf{3}]\cdot 54H_2O$. This is consistent with the greater sensitivity to quenching of the luminescence by coordinated aqua ligands for Eu(III) compared with Tb(III), since the smaller energy gap for the lowest energy transition for Eu(III) renders the vibrational coupling to ν(OH) modes more efficient than for Tb(III).

The solid-state variable temperature emission spectra obtained for the dinuclear terbium compound $H_{0.5}K_{8.5}Na[\mathbf{1}]\cdot 30H_2O$, with excitation wavelengths of 275 and 313 nm, show much weaker luminescence than that observed for compound $K_4Li_4H_4[\mathbf{2}]\cdot 58H_2O$. The spectra obtained at 14 K have features similar to those obtained for $K_4Li_4H_4[\mathbf{2}]\cdot 58H_2O$, with the expected Tb(III) transitions. As the temperature is increased with λ_{ex} = 275 nm, the intensities of all the transitions decrease as per the other compounds; however, at 225 K and above peaks are weak and broadened, consistent with no visible luminescence at room temperature. The temperature-dependent behavior with λ_{ex} = 313 nm is a little more complicated, with all of the transitions decreasing in intensity as the temperature is increased from 14 to 225 K.

As no sensitized Tb(III) emission is detected for **1** at room temperature, we are able to deduce the contribution to the observed luminescence from each metal center in the structurally related octanuclear Tb complex **2**. The lack of room temperature luminescence for **1** suggests that metal centers Tb1 and Tb2, which are present in both **1** and **2**, do not contribute to the luminescence observed for **2**. The center Tb1 has no picolinate ligands, and since the excitation spectrum of **2** has shown that sensitization proceeds only via the organic chromophore at room temperature, and not via the POM, we conclude this metal center is not sensitized and does not contribute to the luminescence. A similar conclusion can be made for Tb2, although a picolinate ligand is coordinated. An analysis of bond angles and coordination geometries for each of the Tb metal centers (Table 1) sheds some light on this effect. Previous work from Yamase et al. has shown that the efficiency of emission is strongly temperature dependent in POM complexes which contain Ln−O−W bond angles of about 150°, since this angle allows for effective electron hopping through fπ-pπ-dπ orbital mixing. The presence of five such (corner-sharing) bond angles to Tb2 (151−161°) in both **1** and **2** facilitates efficient quenching of the emission, through involvement of the Tb(IV)−W(V) charge transfer states.

For compound **2**, we therefore assign the observed biexponential decay components to Tb3 and Tb4. For Tb3, which has three Tb−O−W bonds, two of these are involved in

dx.doi.org/10.1021/ic202349u | Inorg. Chem. 2012, 51, 1142−1151

an edge-shared linkage with smaller Tb−O−W bond angles of 107° and 98°, which will be less efficient for quenching the Tb(III) luminescence. Similarly, for Tb4, there is a single Tb−O−W bond with an angle of 147°, but this is evidently insufficient to completely quench the emission sensitized by the picolinate ligand. On the basis of the room temperature luminescent lifetimes, we assign the long and short-lived lifetime components to Tb3 and Tb4, respectively, because of the presence of three and six inner-sphere aqua ligands that can quench the luminescence.

CONCLUDING REMARKS

The hybrid organic−inorganic molecular species reported herein represent an interface between classical rare earth phosphors and the luminescent lanthanoid coordination complexes that are the focus of much contemporary research. Our synthesis of bulk samples of structurally characterized "ternary" Ln-org-POM complexes has allowed for the first time site-specific determination of the luminescence properties for the different Tb(III) and Eu(III) centers and a delineation of the luminescence-sensitization through both the organic and inorganic ligands. At room temperature both organic picolinate and inorganic POM ligands serve to sensitize the Eu(III) luminescence in complex **3**, following excitation with UV light. Although the luminescence is more intense at 14 K, there is little difference in the temperature dependence observed for sensitization through both types of "antenna". In contrast, at room temperature the Tb(III) luminescence in the Tb analogue **2** is only sensitized through the organic ligand, with the POM becoming an effective inorganic antenna only at low temperature. The observed difference in the temperature dependencies of the sensitization of the Tb(III) luminescence at two distinct excitation wavelengths, that is, through two different antennas, clearly illustrates the importance of distinguishing sensitization pathways in molecular and nanoscale luminophores. Finally, it is clear from this work that Ln-org-POM complexes with improved Ln(III) emissive properties will result from complexes with edge-sharing rather than corner-sharing Ln−O−W linkages and a minimum number of aqua co-ligands on the emitting Ln(III) centers.

ASSOCIATED CONTENT

Supporting Information

X-ray crystallographic files in CIF format for $H_{0.5}K_{8.5}Na$-[**1**]·$30H_2O$, $K_4Li_4H_4$[**2**]·$58H_2O$, and $Eu_{1.66}K_7$[**3**]·$54H_2O$; additional structural figures; infrared spectra; table of selected interatomic distances and angles. This material is available free of charge via the Internet at http://pubs.acs.org.

AUTHOR INFORMATION

Corresponding Author

*E-mail: c.boskovic@unimelb.edu.au.

ACKNOWLEDGMENTS

We thank the Australian Research Council for financial support and Professor R. Leonelli (U. Montréal) for help with the Acton Trivista 500i spectrometer.

REFERENCES

(1) (a) Ronda, C. R.; Justel, T.; Nikol, H. *J. Alloys Cmpd.* **1998**, *275*−*277*, 669. (b) Geng, F.; Ma, R.; Sasaki, T. *Acc. Chem. Res.* **2010**, *43*, 1177. (c) Höppe, H. A. *Angew. Chem., Int. Ed.* **2009**, *48*, 3572.

(2) (a) Bünzli, J.-C. G.; Piguet, C. *Chem. Soc. Rev.* **2005**, *34*, 1048. (b) Moore, E. G.; Samuel, A.; Raymond, K. N. *Acc. Chem. Res.* **2009**, *42*, 542. (c) Bünzli, J.-C. G. *Chem. Rev.* **2010**, *110*, 2729.

(3) (a) Binnemans, K. *Chem. Rev.* **2009**, *109*, 4283. (b) Carlos, L. D.; Ferreira, R. A. S.; de Zea Bermudez, V.; Julián-López, B.; Escribano, P. *Chem. Soc. Rev.* **2011**, *40*, 536.

(4) (a) Pope, M. T. *Heteropoly and Isopoly Oxometalates*; Springer-Verlag: Berlin, Germany, 1983. (b) Borraás-Almenar, J. J.; Coronado, E.; Müller, A.; Pope, M. T., Eds.; *Polyoxometalate Molecular Science*; Kluwer: Dordrecht, The Netherlands, 2003.

(5) Bassil, B. S.; Kortz, U. *Z. Anorg. Allg. Chem.* **2010**, *636*, 2222.

(6) (a) Boglio, C.; Lemière, G.; Hasenknopf, B.; Thorimbert, S.; Lacôte, E.; Malacria, M. *Angew. Chem., Int. Ed.* **2006**, *45*, 3324. (b) Kholdeeva, O. A.; Timofeeva, M. N.; Maksimov, G. M.; Maksimovskaya, R. I.; Neiwert, W. A.; Hill, C. L. *Inorg. Chem.* **2005**, *44*, 666. (c) Han, J. W.; Hill, C. L. *J. Am. Chem. Soc.* **2007**, *129*, 15094.

(7) (a) Al Damen, M. A.; Clemente-Juan, J. M.; Coronado, E.; Martí-Gastaldo, C.; Gaita-Ariño, A. *J. Am. Chem. Soc.* **2008**, *130*, 8874. (b) Al Damen, M. A.; Cardona-Serra, S.; Clemente-Juan, J. M.; Coronado, E.; Gaita-Arino, Marti-Gastaldo, C.; A.; Luis, F.; Montero, O. *Inorg. Chem.* **2009**, *48*, 3467.

(8) Ritchie, C.; Speldrich, M.; Gable, R. W.; Sorace, L.; Kögerler, P.; Boskovic, C. *Inorg. Chem.* **2011**, *50*, 7004.

(9) Ritchie, C.; Moore, E. G.; Speldrich, M.; Kögerler, P.; Boskovic, C. *Angew. Chemie Int. Ed.* **2010**, *49*, 7702.

(10) (a) Yamase, T. *Chem. Rev.* **1998**, *98*, 307. (b) Yamase, T. In *Handbook on the Physics and Chemistry of Rare Earths*; Gschneider, K. A., Jr., Bünzli, J.-C. G., Pecharsky, V. K., Eds.; Elsevier Science: New York, 2009; Vol. *39*, pp 297−354.

(11) Yamase, T.; Kobayashi, T.; Sugeta, M.; Naruke, H. *J. Phys. Chem. A.* **1997**, *101*, 5046.

(12) Ozeki, T.; Yamase, T. *J. Alloys Compd.* **1993**, *192*, 28.

(13) (a) Zhang, C.; Howell, R. C.; McGregor, D.; Bensaid, L.; Rahyab, S.; Nayshtut, M.; Lekperic, S.; Francesconi, L. C. *C. R. Chim.* **2005**, *8*, 1035. (b) Boglio, C.; Lenoble, G.; Duhayon, C.; Hasenknopf, B.; Thouvenot, R.; Zhang, C.; Howell, R. C.; Burton-Pye, B. P.; Francesconi, L. C.; Lacôte, E.; Thorimbert, S.; Malacria, M.; Afonso, C.; Tabet, J.-C. *Inorg. Chem.* **2006**, *45*, 1389. (c) Burton-Pye, B. P.; Francesconi, L. C. *Dalton Trans.* **2011**, *40*, 4421.

(14) Rodrigues, M. J. E.; Paz, F. A. A; Sá Ferreira, R. A.; Carlos, L. D.; Nogueira, H. I. S. *Mater. Sci. Forum* **2006**, *514*−*516*, 1306.

(15) Granadeiro, C. M.; Sá Ferreira, R. A.; Soares-Santos, P. C. R.; Carlos, L. D.; Nogueira, H. I. S. *J. Alloys Cmpd.* **2008**, *451*, 422.

(16) Lu, Y.; Li, Y.; Wang, E.; Xu, X.; Ma, Y. *Inorg. Chim. Acta* **2007**, *360*, 2063.

(17) (a) Hussain, F.; Gable, R. W.; Speldrich, M.; Kögerler, P.; Boskovic, C. *Chem. Commun.* **2009**, 328. (b) Ritchie, C.; Boskovic, C. *Cryst. Growth Des.* **2010**, *10*, 488. (c) Ritchie, C.; Miller, C. E.; Boskovic, C. *Dalton Trans.* **2011**, *40*, 12037.

(18) Kortz, U.; Savelieff, M. G.; Bassil, B. S.; Dickman, M. H. *Angew. Chem., Int. Ed.* **2001**, *40*, 33.

(19) Pope M. T. *Compr. Coord. Chem. II* **2004**, *4*, 635, and references therein.

(20) (a) Bassil, B. S.; Kortz U. *Dalton Trans.* **2011**, *40*, 9649, and references therein. (b) Lisnard, L.; Dolbecq, A.; Mialane, P.; Marrot, J.; Codjovi, E.; Secheresse, F. *Dalton Trans.* **2005**, 3913.

(21) Dolbecq, A.; Dumas, E.; Mayer, C. R.; Mialane, P. *Chem. Rev.* **2010**, *110*, 6009, and references therein.

(22) (a) Detusheva, L. G.; Kuznetsova, L. I.; Dovlitova, L. S.; Likholobov, V. A. *Russ. Chem. Bull., Int. Ed.* **2003**, *52*, 370. (b) Craciun, C.; Rusu, D.; Pop-Fanea, L.; Hossu, M.; Rusu, M.; David, L. *J. Radioanal. Nucl. Chem.* **2005**, *264*, 589.

(23) Zolin, V. F.; Puntus, L. N.; Tsaryuk, V. I.; Kudryashova, V. A.; Legendziewicz, J.; Gawryszewska, P.; Szostak, R. *J. Alloys Compd.* **2004**, *380*, 279.

(24) Berry, M. T.; May, P. S.; Xu, H. *J. Phys. Chem.* **1996**, *100*, 9216.

(25) Watson, W. M.; Zerger, R. P.; Yardley, J. T.; Stucky, G. D. *Inorg. Chem.* **1975**, *14*, 2675.

(26) Beeby, A.; Clarkson, I. M.; Dickins, R. S.; Faulkner, S.; Parker, D.; Royle, L.; de Sousa, A. S.; Williams, J. A. G.; Woods, M. *J. Chem. Soc., Perkin Trans. 2* **1999**, *3*, 493.
(27) Rosen, D. L.; Niles, S. *Appl. Spectrosc.* **2001**, *55*, 208.